Optics & Laser Technology 164 (2023) 109548

Contents lists available at ScienceDirect

Optics and Laser Technology

journal homepage: www.elsevier.com/locate/optlastec

Full length article

Generation of diffraction-free Bessel beams based on combined axicons

Chengming Lyu [a], Milivoj R. Belić [b], Yongdong Li [a], Yiqi Zhang [a,*]

[a] Key Laboratory for Physical Electronics and Devices of the Ministry of Education & Shaanxi Key Lab of Information Photonic Technique, School of Electronic and Information Engineering, Xi'an Jiaotong University, Xi'an 710049, China
[b] Science Program, Texas A&M University at Qatar, Doha, P.O. Box 23874, Qatar

ARTICLE INFO

Keywords:
Bessel beams
Diffraction-free
Combined axicon
Angular spectrum reconstruction

ABSTRACT

Bessel beams are of great interest because of their unique diffraction-free properties and broad potential applications. In this paper we investigate the generation of diffraction-free Bessel beams by combined axicons. We found that such beams can propagate up to 9.63 km in free space. Longer propagation distance can be achieved by utilizing the angular spectrum reconstruction theory that is proposed here for the first time, to rectify the distortion caused by diffraction and extend the propagation distance up to 15 km from the emission plane. Additionally, the self-healing property of the Bessel beam is demonstrated by initially removing the main lobe and reconstructing the beam after 9.63 km. Finally, we demonstrate that the Bessel beam has outstanding performance in weak and moderate turbulence atmosphere. The results obtained provide an effective way for optical communication in deep space and may inspire new ideas for wireless energy transmission in the microwave range.

1. Introduction

The diffraction-free beam is a special kind of beams that do not diffract in free space during propagation, and among the first such beams discovered were the Bessel beams [1]. The Bessel beam is a solution of the three-dimensional Helmholtz equation, with field landscape in the transverse plane (x, y) distributed according to the first kind of Bessel functions, where the longitudinal coordinate (z) is the propagation direction. Thanks to their non-diffracting property, a great deal of effort is expended on deep investigation of Bessel beams [2–5]. Szameit's group reported a new class of radially self-accelerated diffractionless beams that evolve in a spiral orbit and maintain amplitude and phase distributions in a rotating stationary frame [2–4]. They also reported a new method for generating long-range self-healing Bessel beams based on a toroidal (annular) lens and a spherical lens in a 4f configuration [5]. Until now, several potential applications of Bessel beams have been proposed, including optical trapping [6,7], laser drilling [8], laser precision collimation [9], optical micromanipulation [10], and wireless energy transmission [11]. Recently, diffraction-free beams passing through an elliptical annular aperture have been shown to produce hollow beams with zero central intensity, which extended the application of Bessel beams [12]. It is worth noting that the propagation trajectory (i.e., the trajectory of the "mass center") of the Bessel beam is a straight line. Besides the non-diffracting property, the Bessel beam is also capable of self-reconstructing its field [13,14] when the part of the beam is blocked by an obstacle, which is known as the self-healing property. Therefore, Bessel beams can tolerate partial obstacle occlusion and still remain an effective solution for realizing long-distance free-space optical communication [15–17]. Additionally, if the paraxial approximation for the Helmholtz equation is considered, which results in the Schrödiner-like equation, Berry and Balazs obtained the Airy non-diffracting wavepacket [18]. Based on this, Christodoulides' group developed finite-energy Airy beams [19,20] that accelerate along a parabolic trajectory, and in this manner opened another page in the history of diffraction-free self-accelerating beams.

As early as 1987, Durnin proposed the ring-slit method for generating approximate Bessel beams at finite apertures that can propagate over considerable distances [1]. Subsequently, computer-generated holograms were proposed to generate Bessel beams, and the diffraction-free distance reached 15.8 m [21]. It was also proposed to convert Gaussian beams generated by the laser into Bessel beams using a conventional axicon lens [22] or volume holographic axicons [23], and soon higher-order Bessel beams of arbitrary order were achieved by illuminating an axicon with appropriate Laguerre–Gaussian (LG) beams [24,25]. In addition, higher-order Bessel beams can also be prepared by using metasurfaces [26–28], diffraction gratings [29], geometric phase-based optical elements [30] and spatial light modulators [31–34]. However, a lot of studies based on Bessel beams can only maintain the diffraction-free property over a short distance, which limits its potential

---

[*] Corresponding author.
E-mail address: zhangyiqi@xjtu.edu.cn (Y. Zhang).

https://doi.org/10.1016/j.optlastec.2023.109548
Received 4 October 2022; Received in revised form 20 March 2023; Accepted 26 April 2023

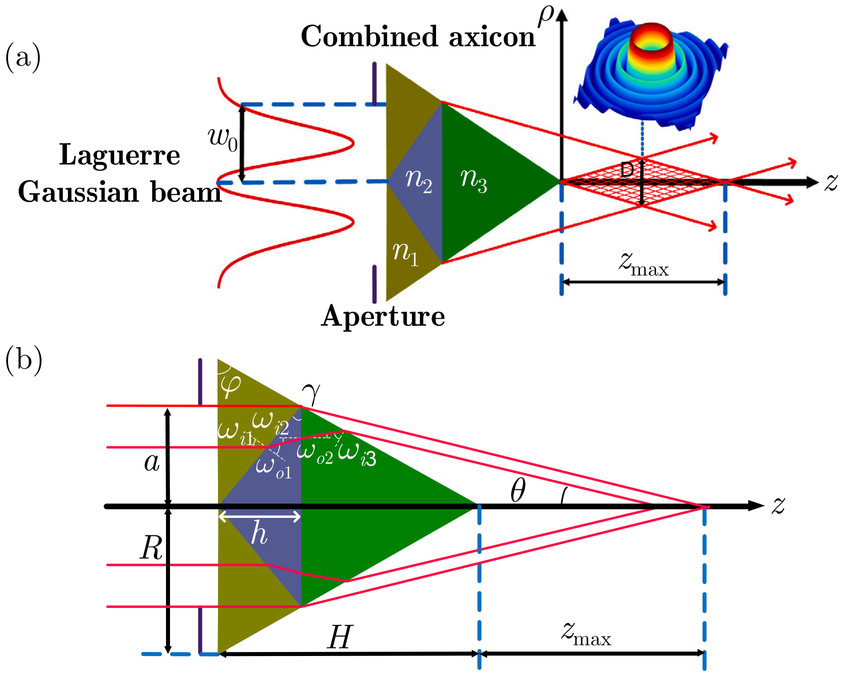

Fig. 1. (a) Scheme for generating long-distance diffraction-free Bessel beams from the combined axicon. (b) Magnified combined axicon model.

engineering applications. As a result, how to prolong the diffraction-free distance to hundreds of meters or even kilometers became a significant issue. It is worth mentioning that the intensity distribution of long-range Bessel beam propagation was investigated [35–40], but the phase distribution carrying the orbital angular momentum that greatly enhances the communication capacity is not received sufficient attention. It will be done in this work.

In this work, we propose a combined axicon model to produce diffraction-free zero-order and higher-order Bessel beams over 9.63 km, by selecting different refractive indices of materials and their different combinations. Proper parameters contribute to the enhancement of the diffraction-free distance. This scheme does not demand an extremely small base angle of the axicon and has a high conversion efficiency. In addition, the structure of the combined axicon is stable. To remediate the distortion caused by diffraction, a method of angular spectral reconstruction is developed, based on the angular spectrum propagation theory [41–43], which allowed further increase of the diffraction-free transmission distance to 15 km. We believe that our results represent one of the effective solutions for obstacle-tolerant links, enabling low intensity restoration of obstructed links in spite of obscured main lobes.

2. Theory

2.1. Generation of higher-order Bessel beams

Bessel beams and LG beams can be linked by an axicon [24], thanks to the fact that axicons can provide conical phase, which is the condition for the formation of a Bessel beam. Therefore, we propose a combined axicon model, as shown in Fig. 1, based on which we obtain long-range diffraction-free Bessel beams from LG beams. The diffractionless Bessel beam is generated in the gridded region of Fig. 1(a), and its optical field is given by

$$u(r,\phi,z) = cJ_l(k_r r)\exp(\mathrm{i}l\phi), \tag{1}$$

where c is the factor corresponding to the longitudinal position $\sqrt{z}$, $\exp(\mathrm{i}l\phi)$ is an azimuthal phase factor, i is imaginary unit, l is the topological charge, $J_l(\cdot)$ is the lth-order Bessel function, and k_r is the longitudinal wave number related to the material and cutting type. The intensity in the transverse plane behind the axicon is

$$I(\rho,\phi,z) = |u(r,\phi,z)|^2 \propto C\left|J_l(k_r r)\right|^2, \tag{2}$$

where C is the factor corresponding to the longitudinal position z. Consequently, the on-axis intensity of this beam increases linearly in the maximum diffraction-free range, and similar results can be also found in [22,24]. It is worth mentioning that the adoption of a phase element [44] or a ring lens [5] can produce an on-axis intensity distribution with smooth and constant intensity. The transverse distribution of a high-order Bessel beam is shown in the inset of Fig. 1(a).

To clearly perceive the combined axicon action and analyze the model conveniently, we depict the details of the combined axicon in Fig. 1(b). According to the laws of refraction and angular equivalence relation, one obtains $n_1\sin\omega_{i1} = n_2\sin\omega_{o1}$, $n_2\sin\omega_{i2} = n_3\sin\omega_{o2}$, $n_3\sin\omega_{i3} = \sin(\varphi+\theta)$ with $\omega_{i1} = \gamma$, $\omega_{i2} = \omega_{o1} - \gamma$, $\omega_{i3} = \varphi - \omega_{o2}$. So, one gets

$$\theta = \arcsin\left[n_3\sin(\varphi-\varphi_t)\right] - \varphi, \tag{3}$$

$$\varphi_t = \arcsin\left\{\frac{n_2}{n_3}\sin\left[\arcsin\left(\frac{n_1\sin(\gamma)}{n_2}\right) - \gamma\right]\right\}, \tag{4}$$

where n_1, n_2, and n_3 are the refractive indices of the three materials respectively, φ is the base angle of combined axicon, R is the radius of the combined axicon, a is the radius of the aperture, H is the height of the combined axicon, and h is the height of the material with refractive index n_2. All these quantities are clearly denoted in Fig. 1(b). As a result, the maximum diffraction-free distance is

$$z_{\max} = \frac{ka}{k_r}, \tag{5}$$

where $k_r = k\sin(\theta)$, and under small angle approximation, $z_{\max} = a/\theta$. Thus, for a given aperture size, the diffraction-free distance depends only on θ. Therefore, a theoretical diffraction-free distance of several kilometers can be reached by reasonably selecting materials with different refractive indices and sizes. The smaller the θ value is, the larger the $z_{\max}$ value will be. From Eq. (3), one observes that θ is 0 and $z_{\max} = \infty$ when $\varphi = \varphi_t$ (this is the limiting case). From Eq. (4), we can find that when φ is determined, the refractive index and the γ value can be reasonably chosen so that φ_t is infinitely close to φ to obtain an awfully small θ and a great $z_{\max}$.

Meanwhile, the combined axicon system has an amplitude transmissivity of 0.8531, according to the Fresnel's law, hence its power conversion efficiency can reach 72%. In addition, we presume that the device can be applied for deep space optical communication, so the loss is negligible.

2.2. Angular spectrum propagation theory

The propagation of a light beam is governed by the wave equation

$$\frac{1}{v^2}\frac{\partial^2\psi}{\partial t^2} = \frac{\partial^2\psi}{\partial x^2} + \frac{\partial^2\psi}{\partial y^2} + \frac{\partial^2\psi}{\partial z^2}, \tag{6}$$

where the speed $v = 1/\sqrt{\mu\epsilon}$, with ϵ being the dielectric permittivity and μ the magnetic permeability of the medium. We assume that the wave function $\psi(x, y, z, t)$ has a complex amplitude $\psi_p(x, y, z)$, which is at the carrier wave frequency ω_0:

$$\psi(x, y, z, t) = \psi_p(x, y, z)\exp\left(i\omega_0 t\right). \tag{7}$$

Substituting Eq. (7) into Eq. (6), one ends up with the Helmholtz equation for ψ_p:

$$\frac{\partial^2\psi_p}{\partial x^2} + \frac{\partial^2\psi_p}{\partial y^2} + \frac{\partial^2\psi_p}{\partial z^2} + k^2\psi_p = 0, \tag{8}$$

where $k = \omega_0/v = 2\pi/\lambda$, with λ being the wavelength in the medium. Taking Fourier transform of Eq. (8), one obtains

$$\frac{d^2\Psi_p}{dz^2} + k_0^2\left(1 - \frac{k_x^2}{k^2} - \frac{k_y^2}{k^2}\right)\Psi_p = 0, \tag{9}$$

where Ψ_p is the Fourier transform of ψ_p. The general solution of Eq. (9) is thus

$$\Psi_p(k_x, k_y; z) = \Psi_{p0}(k_x, k_y)\exp\left(ikz\sqrt{1 - \frac{k_x^2}{k^2} - \frac{k_y^2}{k^2}}\right), \tag{10}$$

where $\Psi_{p0}(k_x, k_y) = \Psi_p(k_x, k_y; z = 0)$ is the Fourier transform of the initial field at $z = 0$.

We consider a linear system with the input $\Psi_{p0}(k_x, k_y)$ and the output $\Psi_p(k_x, k_y; z)$, so that the spatial frequency response of the system is given by

$$\mathcal{H}(k_x, k_y; z) = \frac{\Psi_p(k_x, k_y; z)}{\Psi_{p0}(k_x, k_y)} = \exp\left[ikz\sqrt{1 - \left(\lambda f_x\right)^2 - (\lambda f_y)^2}\right], \tag{11}$$

with $f_x^2 + f_y^2 < 1/\lambda^2$. We refer to $\mathcal{H}$ as the spatial frequency transfer function at the position z to which the light has traveled in the medium. Under the Fresnel approximation [45],

$$\mathcal{H} = e^{ikz}\exp\left[-i\pi\lambda z\left(f_x^2 + f_y^2\right)\right].$$

The field distribution at z in the real space is finally recast as

$$\psi_p = \mathcal{F}^{-1}\left\{\mathcal{F}\{\psi_{p0}(x, y)\}\cdot\mathcal{H}(k_x, k_y; z)\right\}, \tag{12}$$

where $\mathcal{F}$ and $\mathcal{F}^{-1}$ are the Fourier transform operator and its inverse, respectively. In numerical simulations, it is important to add a guard area to prevent spectral aliasing [45], which is set to 6.4 m to prevent the numerical artifacts that occur at long propagation distances. It is worth noting that this is just a strategy adopted to address numerical artifacts caused by discrete sampling. In reality, there is no issue of numerical artifacts.

2.3. Atmospheric turbulence

Table 1
Comparison between theoretical and numerical beam waists.

Order	Theory (mm)	Simulation (mm)
$l = 0$	5.49	5.47
$l = 1$	13.50	14.06
$l = 2$	19.80	19.50
$l = 3$	25.68	25.05
$l = 4$	31.36	30.47

The refractive index fluctuations caused by turbulence during beam transmission in the atmosphere can distort the amplitude and phase of the beam. Multi-phase masks are generally utilized to simulate atmospheric turbulence [46–48]. The turbulence model developed by von Karman and Tatarski is adopted in our simulation, and the fluctuation spectrum of the refractive index can be represented as [35,49,50]

$$\phi_n(\kappa) = 0.033C_n^2\exp\left(-\frac{\kappa^2}{\kappa_m^2}\right)\left(\kappa^2 + \kappa_0^2\right)^{-11/6}, \tag{13}$$

where κ is the angular spatial frequency, C_n^2 is refractive index structure parameter which represents the strength level of turbulence is, $\kappa_0 = 2\pi/L_0$ and $\kappa_m = 5.92/l_0$. L_0 and l_0 are the outer and inner scale of turbulence, respectively.

As shown in Fig. 3, atmospheric turbulence is simulated by inserting random phase masks is along the beam propagation path. The relation between the phase spectrum and the fluctuation spectrum of refractive index is [50]

$$\Phi(\kappa) = 2\pi k^2\Delta z\phi_n(\kappa), \tag{14}$$

where Δz denotes the distance between the two phase masks.

The phase distribution in atmospheric turbulence can be obtained by [50]

$$\varphi(x, y) = \mathcal{F}\left[C\cdot\left(\frac{2\pi}{N\Delta x}\right)\cdot\sqrt{\Phi(\kappa)}\right], \tag{15}$$

where N and Δx are the number of sampling points and the grid interval of the phase mask, respectively. C is a $N\times N$ array of complex random numbers with zero mean and variance 1.

3. Results

3.1. Generated Bessel beams

Next, we consider Bessel beams generated from LG beams by the procedure described above. The parameters for generating the Bessel beams of different orders, by using the combined axicon model, are as follows: $n_1 = 2.407$, $n_2 = 1.600$, $n_3 = 1.820$, $\varphi = 4.78°$, $\gamma = 4.78°$, $R = 400$ mm, $a = 200$ mm, $\lambda = 632.8$ nm. The incident LG beams are shown in Fig. 2(a), with the corresponding phase distributions given in Fig. 2(b). Note that the beam waists of LG beams from the 0-order to the 4th order are chosen as 200 mm, 160 mm, 130 mm, 110 mm and 100 mm, respectively. Across the combined axicon, the amplitude profiles of the LG beams do not change, however the phases are modulated, as shown in Fig. 2(c). The generated Bessel beams at $z = 5$ km are shown in Fig. 2(d) and the corresponding phases in Fig. 2(e). Note that panels in (d) and (e) are shown in the window $-100\text{ mm} \le x, y \le 100\text{ mm}$ due to the restrictions of the coherent area.

In Table 1, we compare beam waists of the main lobe (ring) of Bessel beams obtained directly from Eq. (1) and based on the model proposed in this work, which are listed in the left column (theory) and the right column (simulation), respectively. One finds that our results are in remarkable compliance with the theoretical results, which clearly demonstrates the validity of the model.

The intensity and phase distributions of the Bessel beam at $z = 9.63$ km, which is the diffraction-free limit, are illustrated in Figs. 4(a) and 4(b). One can observe that the Bessel beams of different orders can maintain their shape after a long propagation distance. Fig. 4(c) presents the variation of beam waists during propagation. It is apparent that the Bessel beam produced by the combined axicon exhibits excellent diffraction-free properties and its beam waist is practically

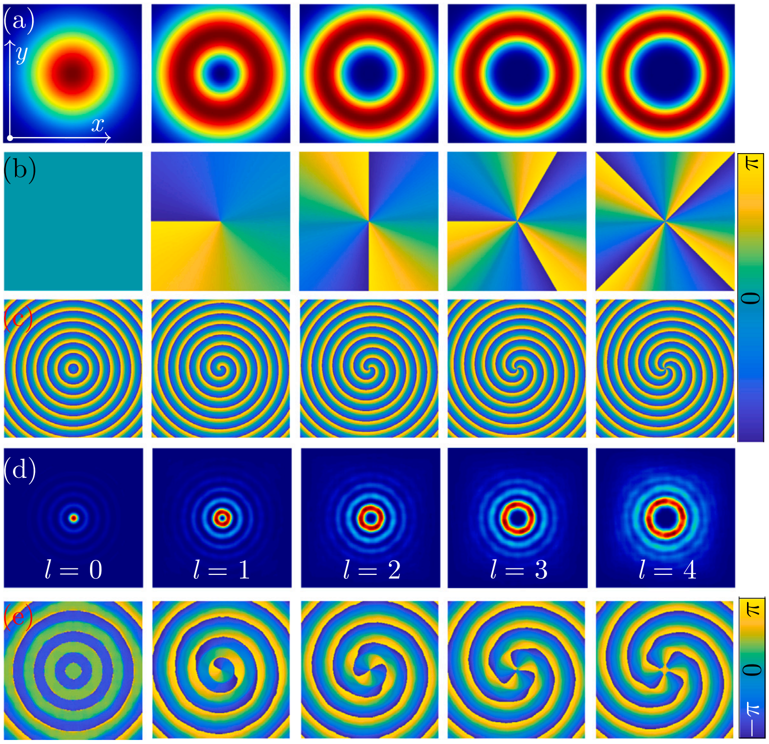

Fig. 2. (a) Intensity distributions of the input LG beams with different orders. (b) Phase distributions corresponding to (a). (c) Phases of the beams across the combined axicon. (d) Generated Bessel beams at $z = 5$ km. (e) Phase distributions corresponding to (d). Panels in (a)–(c) are shown in the window -200 mm $\leq x, y \leq 200$ mm. Panels in (d) and (e) are shown in the window -100 mm $\leq x, y \leq 100$ mm.

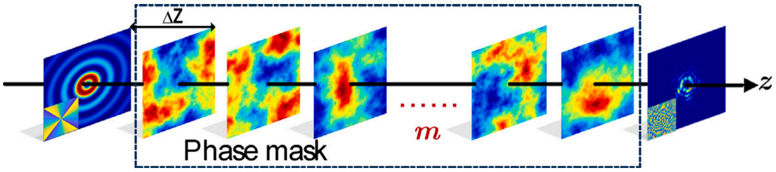

Fig. 3. Propagation model of a Bessel beam in atmospheric turbulence.

non-expanding, while the Gaussian beam with the same beam waist will expand by a factor of 64 ($l = 0$), 10 ($l = 1$), 5 ($l = 2$), 3 ($l = 3$), and 2 ($l = 4$) times, respectively. Note that the curves in Fig. 4(c) start from ∼253 m ($l = 0$), ∼1.52 km ($l = 1$), ∼3.16 km ($l = 2$), ∼4.05 km ($l = 3$), ∼4.18 km ($l = 4$), which are defined as the minimum propagation distances z_p, the reason being that the LG beam does not directly transform into the Bessel beam immediately after passing through the combined axicon. As shown in Fig. 1, the Bessel beam gets established in the coherence (gridded) region, which is a bit away from the combined axicon. As shown in Fig. 4(d), Bessel beams with different topological charge l have different z_p. Moreover, the smaller l is, the smaller z_p will be. In addition, z_p shows a positive correlation with the beam waist w of LG beams. If l is determined, decreasing w can reduce z_p. However, the value of w should not be too small to reach a sufficiently long diffraction-free distance. As an example, when $l = 1$ and $w = 60$ mm, the Bessel beam is generated at 1.01 km, but it starts to broaden after $z = 5.06$ km (not shown). On the other hand, if w is extremely small, the Bessel beam cannot be generated.

3.2. Angular spectrum reconstruction

According to Eqs. (3)–(5), the maximum diffraction-free distance of the Bessel beam generated by the combined axicon will be $z_{\max} = 9.63$ km. It will pose a great challenge on the selection of parameters of the combined axicon to further extend the diffraction-free distance. On one hand, the angular error must be extremely small, and on the other, the selection of the material will get complicated. Here, we will show how to extend the diffraction-free propagation distance by applying the method of angular spectrum reconstruction.

We define the angular spectrum reconstruction factor as

$$S(k_x, k_y; z_d) = \exp\left(-\mathrm{i}kz_d\sqrt{1-(\lambda f_x)^2-(\lambda f_y)^2}\right),$$

where z_d refers to the desired reconstruction distance. The reconstructed field at the receiving terminal will be

$$\Psi_{p2}(k_x, k_y; z) = S(k_x, k_y; z)\cdot\mathcal{F}_{xy}\{\psi_{p1}\},$$

where ψ_{p1} is the field distribution of the beam at the receiver. It is fairly easy to implement this system by utilizing Fourier transformation with a lens and then changing the phase by the spatial light modulator. Note that

$$\psi_{p1} \neq \mathcal{F}_{xy}^{-1}\left\{\mathcal{H}\cdot\mathcal{F}_{xy}\{\psi_{p0}\}\right\}.$$

In order to ensure the accuracy of the simulation, the calculation window is enlarged twice, to provide a large enough free space for the propagation, however the scale of the receiver does not change. In Fig. 5, the red boxes indicate the receiver size, outside which the information is lost.

In Fig. 5(a), the intensity distribution of Bessel beams of different orders are displayed after propagating for $z = 15$ km in free space.

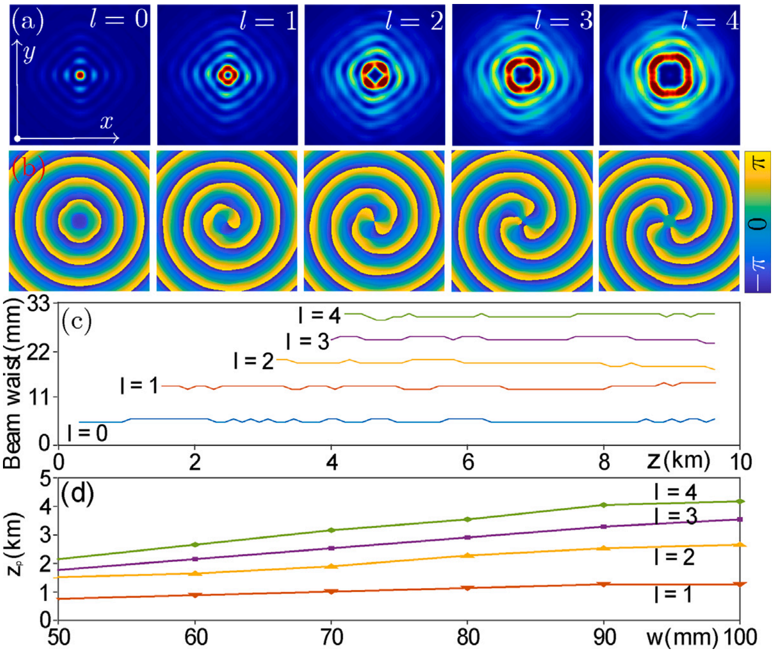

Fig. 4. (a) Intensity distributions of Bessel beams at the theoretical diffraction-free limit $z = 9.63\,\mathrm{km}$. (b) Phase distributions corresponding to (a). All panels are shown in the window $-100\ \mathrm{mm} \leq x, y \leq 100\ \mathrm{mm}$. (c) Beam waists of different Bessel beams during propagation with different w fixed. (d) Relationship between the minimum propagation distance z_p and w for Bessel beams with different topological charge l.

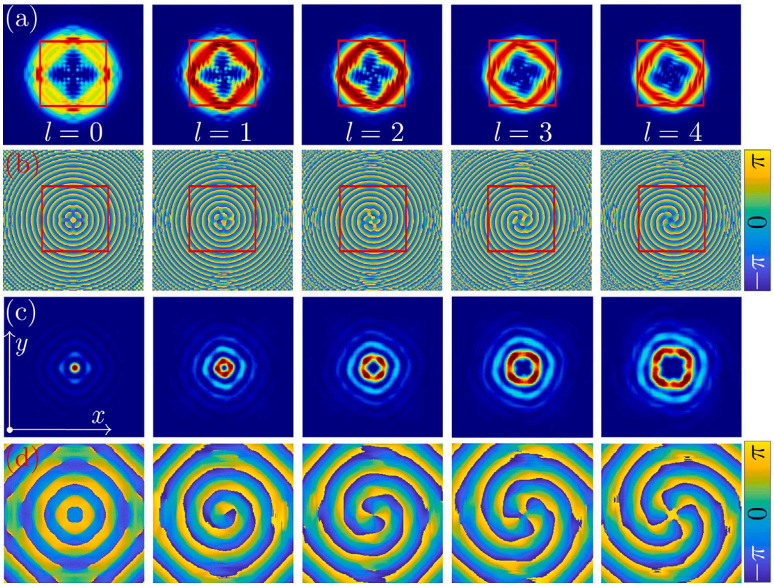

Fig. 5. (a) Intensity distributions of Bessel beams after 15 km propagation in free space. (b) The corresponding phase distributions. (c) Intensity distributions of the reconstructed Bessel beams. (d) The corresponding phase distributions. Panels in (a) and (b) are shown in the window $-400\ \mathrm{mm} \leq x, y \leq 400\ \mathrm{mm}$, while the red boxes are in the window$-200\ \mathrm{mm} \leq x, y \leq 200\ \mathrm{mm}$. Panels in (c) and (d) are shown in the window $-100\ \mathrm{mm} \leq x, y \leq 100\ \mathrm{mm}$.

Clearly, the Bessel beam undergoes a huge spreading and distortion compared to that at $z = 9.63$ km shown in Fig. 4(a). At the same time, the corresponding phase distribution in Fig. 4(b) turns out to be chaotic-like and one can hardly recognize the topological charge. After dense numerical simulations, we obtain an optimized reconstruction distance factor of $z_d = 9000$. The intensity and phase distributions at $z = 15$ km and after reconstruction are shown in Figs. 5(c) and 5(d), in which the distortion is effectively eliminated and the correct l value can be simply extracted from the phase. Consequently, the angular spectrum reconstruction can enhance the performance of our Bessel beam generation procedure in a visible way. It is worth emphasizing that this method is not “created out of nothing” but out of the well grounded theoretical rearrangement of light field in the receiving plane. If the intensity distribution is much larger than the observation plane (the red box) and much of information is lost (e.g., by propagating the beam further up, to say $z = 20$ km), this method will fail to successfully restore the Bessel beams. So, the propagation distance cannot be raised

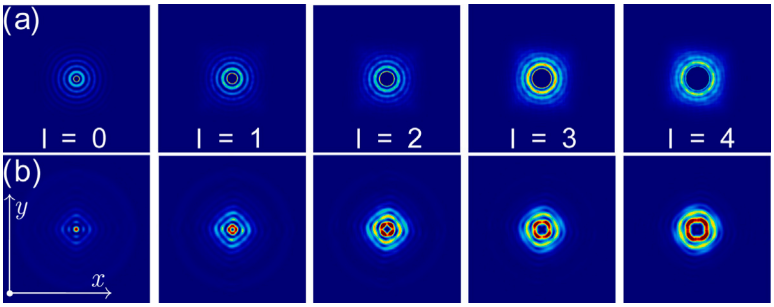

Fig. 6. (a) Bessel beams after removing the main lobe at $z = 5$ km. (b) The same Bessel beams after self-healing, observed at $z = 9.63$ km. All panels are shown in the window -200 mm $\leq x, y \leq 200$ mm. Note in particular the reconstruction of the main lobe, the red ring.

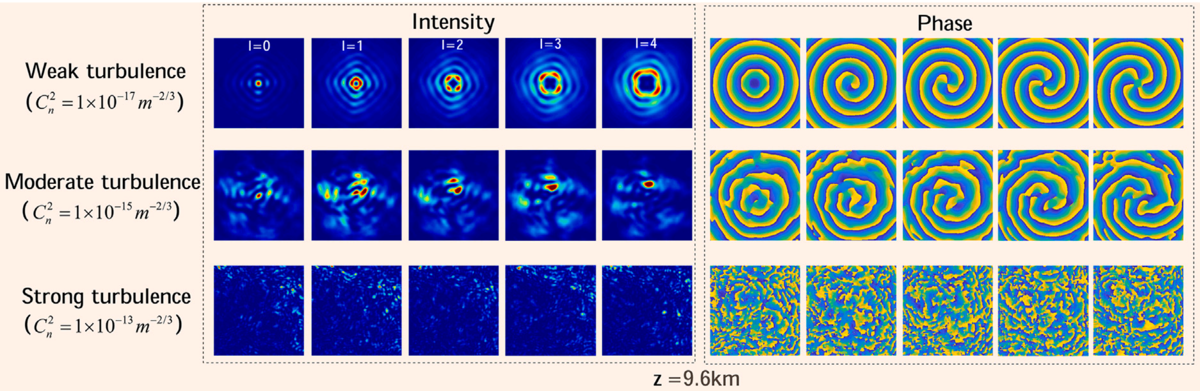

Fig. 7. Intensity and phase distribution of the Bessel beam at $z = 9.6$ km considering turbulence of different strength levels. All Panels are shown in the window -100 mm $\leq x, y \leq 100$ mm.

indefinitely for a given observation plane, unless the plane is enlarged accordingly.

3.3. Self-healing property

One of the remarkable properties of diffraction-free beams is their self-healing property [51], and this is also feasible for the Bessel beam. The intensity distribution of Bessel beams after removing the main lobe (ring) are shown in Fig. 6(a). After propagating to $z = 9.63$ km, the intensity distributions are shown in Fig. 6(b), which are quite similar to those in Fig. 4 — the main lobes are repaired with the energy coming from the side lobes, and this demonstrates the self-healing property of the Bessel beams discussed here.

Last but not least, we would like to note that the reconstruction distance is weakly affected by l. To illustrate this property, in the **Supplemental Materials** we provide an animation that is corresponding to Fig. 6.

3.4. Bessel beams propagate through turbulence

Since our goal is to investigate free-space optical communication systems for deep space (without considering turbulence effects), a proper discussion of atmospheric turbulence at low altitudes is necessary to expand the communication area as well as to extend the application range of this system. One is simulated at three different turbulence strength levels where the structural parameters of refractive index C_n^2 were 1×10^{-13} $\mathrm{m}^{-2/3}$ (strong turbulence), 1×10^{-15} $\mathrm{m}^{-2/3}$ (moderate turbulence), and 1×10^{-17} $\mathrm{m}^{-2/3}$ (weak turbulence). The parameters are kept constant except for the structural parameters. The inner scale of turbulence $l_0 = 0.01$ m, the outer scale $L_0 = 50$ m, the wavelength of Bessel beams $\lambda = 632.8$ nm, the phase mask size is 0.4 m and $N = 512$. The distance between phase masks $\Delta z = 100$ m, and the number of repetitions m is taken as 96. Based on the above parameters, the intensity and phase distributions at $z = 9.6$ km for different turbulence strength levels are shown in Fig. 7. Comparing with Figs. 4(a)–(b), the distributions are almost without change under weak turbulent disturbance. Under moderate turbulent disturbances, the intensity distribution of the Bessel beam tends to lose its profile. The corresponding phase shows distortion, however one still can extract the correct topological charge value. Under strong turbulent disturbances, both distributions are extremely chaotic, rendering it hard to extract the correct information. Some possible solutions are the employment of adaptive optics or deep learning, which is beyond the scope of this work.

4. Conclusion

Summarizing, we have proposed a combined axicon scheme for generating long-range (∼9.63 km) diffractionless Bessel beams. Thanks to the angular spectrum reconstruction method, the diffraction-free distance can be extended up to 15 km. The self-healing property of Bessel beams is also demonstrated. Finally, multi-phase masks are applied to simulate atmospheric turbulence to verify that this beam propagates with little loss of information in weak as well as moderate turbulence. The resulting Bessel beam can serve as an appropriate information carrier for long-range communication, since the intensity distortion due to diffraction can be efficiently suppressed.

Declaration of competing interest

Authors declare that they have no conflict of interest.

Funding

National Natural Science Foundation of China (12074308, U1537210). Work at Texas A&M University at Qatar is supported by the NPRP 13S-0121-200126 project from the Qatar National Research Fund, Qatar (a member of Qatar Foundation).

Data availability

Data will be made available on request.

Appendix A. Supplementary data

Supplementary material related to this article can be found online at https://doi.org/10.1016/j.optlastec.2023.109548.

References

[1] J. Durnin, J.J. Miceli, J.H. Eberly, Diffraction-free beams, Phys. Rev. Lett. 58 (1987) 1499–1501.

[2] C. Vetter, T. Eichelkraut, M. Ornigotti, A. Szameit, Generalized radially self-accelerating helicon beams, Phys. Rev. Lett. 113 (2014) 183901.

[3] C. Vetter, T. Eichelkraut, M. Ornigotti, A. Szameit, Optimization and control of two-component radially self-accelerating beams, Appl. Phys. Lett. 107 (21) (2015) 211104.

[4] M. Ornigotti, A. Szameit, Radially self-accelerating optical pulses, Phys. Rev. A 99 (2019) 023859.

[5] C. Vetter, R. Steinkopf, K. Bergner, M. Ornigotti, S. Nolte, H. Gross, A. Szameit, Realization of free-space long-distance self-healing Bessel beams, Laser Photon Rev. 13 (10) (2019) 1900103.

[6] A.S. Desyatnikov, V.G. Shvedov, A.V. Rode, W. Krolikowski, Y.S. Kivshar, Photophoretic manipulation of absorbing aerosol particles with vortex beams: theory versus experiment, Opt. Express 17 (10) (2009) 8201–8211.

[7] J.C.H. Spence, G. Subramanian, P. Musumeci, Hollow cone illumination for fast TEM, and outrunning damage with electrons, J. Phys. B 48 (21) (2015) 214003.

[8] Y. Matsuoka, Y. Kizuka, T. Inoue, The characteristics of laser micro drilling using a Bessel beam, Appl. Phys. A 84 (4) (2006) 423–430.

[9] M. Duocastella, C. Arnold, Bessel and annular beams for materials processing, Laser Photonics Rev. 6 (5) (2012) 607–621.

[10] D. McGloin, V. Garcés-Chávez, K. Dholakia, Interfering Bessel beams for optical micromanipulation, Opt. Lett. 28 (8) (2003) 657–659.

[11] J.D. Heebl, M. Ettorre, A. Grbic, Wireless links in the radiative near field via Bessel beams, Phys. Rev. A 6 (2016) 034018.

[12] X.-X. Xie, S.-C. Wang, F.-T. Wu, Diffraction optical field of the Bessel beam through elliptical annular aperture, Acta Phys. Sin. 64 (12) (2015) 124201.

[13] V. Garcés-Chávez, D. McGloin, H. Melville, W. Sibbett, K. Dholakia, Simultaneous micromanipulation in multiple planes using a self-reconstructing light beam, Nature 419 (6903) (2002) 145–147.

[14] A. Gatto, M. Tacca, P. Martelli, P. Boffi, M. Martinelli, Free-space orbital angular momentum division multiplexing with Bessel beams, J. Opt. 13 (6) (2011) 064018.

[15] N. Bozinovic, Y. Yue, Y. Ren, M. Tur, P. Kristensen, H. Huang, A.E. Willner, S. Ramachandran, Terabit-scale orbital angular momentum mode division multiplexing in fibers, Science 340 (6140) (2013) 1545–1548.

[16] J. Wang, J.-Y. Yang, I.M. Fazal, N. Ahmed, Y. Yan, H. Huang, Y. Ren, Y. Yue, S. Dolinar, M. Tur, A.E. Willner, Terabit free-space data transmission employing orbital angular momentum multiplexing, Nature Photon. 6 (7) (2012) 488–496.

[17] Y. Yan, G. Xie, M.P.J. Lavery, H. Huang, N. Ahmed, C. Bao, Y. Ren, Y. Cao, L. Li, Z. Zhao, A.F. Molisch, M. Tur, M.J. Padgett, A.E. Willner, High-capacity millimetre-wave communications with orbital angular momentum multiplexing, Nature Commun. 5 (1) (2014) 4876.

[18] M.V. Berry, N.L. Balazs, Nonspreading wave packets, Amer. J. Phys. 47 (1979) 264–267.

[19] G.A. Siviloglou, D.N. Christodoulides, Accelerating finite energy airy beams, Opt. Lett. 32 (8) (2007) 979–981.

[20] G.A. Siviloglou, J. Broky, A. Dogariu, D.N. Christodoulides, Observation of accelerating Airy beams, Phys. Rev. Lett. 99 (2007) 213901.

[21] A. Vasara, J. Turunen, A.T. Friberg, Realization of general nondiffracting beams with computer-generated holograms, J. Opt. Soc. Amer. A 6 (11) (1989) 1748–1754.

[22] G. Scott, N. McArdle, Efficient generation of nearly diffraction-free beams using an axicon, Opt. Eng. 31 (12) (1992) 2640–2643.

[23] A.J. Asuncion, R.A. Guerrero, Generating superimposed bessel beams with a volume holographic axicon, Appl. Opt. 56 (14) (2017) 4206–4212.

[24] J. Arlt, K. Dholakia, Generation of high-order Bessel beams by use of an axicon, Opt. Commun. 177 (1) (2000) 297–301.

[25] V. Jarutis, R. Paškauskas, A. Stabinis, Focusing of Laguerre–Gaussian beams by axicon, Opt. Commun. 184 (1) (2000) 105–112.

[26] Q. Feng, Y. Lin, M. Shan, Y. Mu, L. Li, Generation and measurement of a Bessel vortex beam carrying multiple orbital-angular-momentum modes through a reflective metasurface in the rf domain, Phys. Rev. A 15 (2021) 064044.

[27] J. Wen, L. Chen, X. Chen, S. Kanwal, L. Zhang, S. Zhuang, D. Zhang, D. Lei, Use of dielectric metasurfaces to generate deep-subwavelength nondiffractive Bessel-like beams with arbitrary trajectories and ultralarge deflection, Laser Photon Rev. 15 (5) (2021) 2000487.

[28] X. Meng, X. Chen, R. Chen, H. Li, T. Qu, A. Zhang, Generation of multiple high-order Bessel beams carrying different orbital-angular-momentum modes through an anisotropic holographic impedance metasurface, Phys. Rev. A 16 (2021) 044063.

[29] N. Jiménez, R. Picó, V. Sánchez-Morcillo, V. Romero-García, L.M. García-Raffi, K. Staliunas, Formation of high-order acoustic Bessel beams by spiral diffraction gratings, Phys. Rev. E 94 (2016) 053004.

[30] J. Baltrukonis, O Ulčinas, S. Orlov, V. Jukna, High-order vector Bessel-Gauss beams for laser micromachining of transparent materials, Phys. Rev. Appl. 16 (2021) 034001.

[31] N. Chattrapiban, E.A. Rogers, D. Cofield, I. Wendell T. Hill, R. Roy, Generation of nondiffracting Bessel beams by use of a spatial light modulator, Opt. Lett. 28 (22) (2003) 2183–2185.

[32] S.H. Tao, W.M. Lee, X.-C. Yuan, Dynamic optical manipulation with a higher-order fractional Bessel beam generated from a spatial light modulator, Opt. Lett. 28 (20) (2003) 1867–1869.

[33] J. Wu, Z. Wu, Y. He, A. Yu, Z. Zhang, Z. Wen, G. Chen, Creating a nondiffracting beam with sub-diffraction size by a phase spatial light modulator, Opt. Express 25 (6) (2017) 6274–6282.

[34] R. Bowman, N. Muller, X. Zambrana-Puyalto, O. Jedrkiewicz, P. Di Trapani, M.J. Padgett, Efficient generation of Bessel beam arrays by means of an SLM, Eur. Phys. J. Spec. Top. 199 (1) (2011) 159–166.

[35] P. Birch, I. Ituen, R. Young, C. Chatwin, Long-distance Bessel beam propagation through Kolmogorov turbulence, J. Opt. Soc. Amer. A 32 (11) (2015) 2066–2073.

[36] W. Wanjun, W. Zhensen, S. Qingchao, B. Lu, Propagation of Bessel Gaussian beams through non-Kolmogorov turbulence based on Rytov theory, Opt. Express 26 (17) (2018) 21712–21724.

[37] T. Aruga, H. Kunimori, S. Yoshikado, Generation of a nondiffracting light beam for a long range, AIP Conf. Proc. 702 (1) (2004) 334–341.

[38] Z. Zhang, X. Liang, M. Goutsoulas, N. Efremidis, Z. Chen, Demonstration of turbulence-resistant propagation of anti-diffracting optical beams beyond kilometer distances, in: 2019 Conference on Lasers and Electro-Optics, CLEO, 2019, pp. 1–2.

[39] B.-S. Chen, J.-X. Pu, Propagation of Gauss–Bessel beams in turbulent atmosphere, Chin. Phys. B 18 (3) (2009) 1033.

[40] H.T. Eyyuboğlu, Propagation of higher order Bessel-Gaussian beams in turbulence, Appl. Phys. B 88 (2) (2007) 259–265.

[41] J.W. Goodman, Introduction To Fourier Optics, fourth ed., W.H. Freeman and Company, 2017.

[42] K. Matsushima, T. Shimobaba, Band-limited angular spectrum method for numerical simulation of free-space propagation in far and near fields, Opt. Express 17 (22) (2009) 19662–19673.

[43] T. Kozacki, K. Falaggis, Angular spectrum-based wave-propagation method with compact space bandwidth for large propagation distances, Opt. Lett. 40 (14) (2015) 3420–3423.

[44] P. Gotovski, P. Šlevas, S. Orlov, O. Ulčinas, A. Urbas, Generation of an optical needle beam with a laser inscribed Pancharatnam-Berry phase element under imperfect conditions, Opt. Express 29 (21) (2021) 33331–33345.

[45] D.G. Voelz, Computational Fourier optics, in: A MATLAB Tutorial, SPIE Press, 2011.

[46] A.D. McAulay, Generating Kolmogorov phase screens for modeling optical turbulence, in: T.D. Steiner, P.H. Merritt (Eds.), Laser Weapons Technology, Vol. 4034, International Society for Optics and Photonics, SPIE, 2000, pp. 50–57.

[47] R. Frehlich, Simulation of laser propagation in a turbulent atmosphere, Appl. Opt. 39 (3) (2000) 393–397.

[48] E. Jera, Numerical simulation of Gaussian beam propagation through Kolmogorov phase screen, in: H. Hemmati, D.M. Boroson (Eds.), Free-Space Laser Communications XXXIII, Vol. 11678, International Society for Optics and Photonics, SPIE, 2021, 1167813.

[49] W. Cheng, J.W. Haus, Q. Zhan, Propagation of vector vortex beams through a turbulent atmosphere, Opt. Express 17 (20) (2009) 17829–17836.

[50] S. Fu, C. Gao, Influences of atmospheric turbulence effects on the orbital angular momentum spectra of vortex beams, Photon. Res. 4 (5) (2016) B1–B4.

[51] N.K. Efremidis, Z. Chen, M. Segev, D.N. Christodoulides, Airy beams and accelerating waves: an overview of recent advances, Optica 6 (5) (2019) 686–701.